Chemiresistive Sensing of Volatile Organic Compounds with Films of Surfactant-Stabilized Gold and Gold–Silver Alloy Nanoparticles

Francisco J. Ibañez and Francis P. Zamborini*

Department of Chemistry, University of Louisville, Louisville, Kentucky 40292

ABSTRACT Here we describe the chemiresistive sensing of volatile organic compounds (VOCs) with films of chemically synthesized ~4 nm diameter Au and AuAg alloy nanoparticles (NPs) stabilized by a surfactant, tetraoctylammonium bromide (TOABr). The chemiresistive sensing properties were measured over a concentration range of 100 to 0.04% saturation for methanol (MeOH), ethanol (EtOH), 2-propanol (IPA), and toluene (Tol) vapor analytes and compared directly to the chemiresistive sensing properties of films of 1.6 nm diameter hexanethiolate (C6S)-coated Au monolayer-protected clusters (MPCs). Films of TOABr-stabilized Au NPs exhibit the opposite response compared to those of C6S-coated Au MPCs. The details are unclear, but the mechanism likely involves changes in capacitive charging in the film or improved conductive pathways through the Au NPs upon incorporation of VOCs into the film for the former as opposed to the well-known change in electron hopping conductivity for the latter. This leads to a decrease in resistance in the presence of VOCs for TOABr Au as opposed to an increase for C6S Au. The TOABr Au sensors are more sensitive, especially for polar analytes, and have greater long-term stability compared to C6S Au. The limit of detection (LOD) for films of TOABr-coated Au NPs is 3, 2, 12, and 37 ppm for IPA, MeOH, EtOH, and Tol, respectively, as compared to 106, 326, 242, and 48 for C6S Au. Films of TOABr-stabilized AuAg alloy NPs exhibit the same type of response, but the sensitivity decreases dramatically with increasing Ag content, showing that the metal composition of the NPs in the film plays a role in the sensing properties, which has not been well-recognized in the literature.

KEYWORDS: Au · nanoparticles · films · chemiresistors · sensors · vapors

The detection of volatile organic compounds (VOCs) is important for numerous applications, including public safety,[1,2] environmental protection,[3,4] homeland security,[5] and medical diagnostics.[6] Miniaturized devices capable of sensing VOCs, often termed "electronic noses",[2,7–11] are highly desirable because of their simplicity, portability, and low cost compared to gas chromatography–mass spectrometry (GC–MS) instruments. The goal is to develop hand-held, portable sensors that are capable of identifying and quantifying all of the components, or at least the analyte of interest, in a complex mixture. Strategies involving sensor arrays combined with principle component analysis have shown promise for achieving this important goal.[7,12–14] Several transduction methods have been used in the design of VOC sensors, including piezoelectric,[12,13,15–17] colorimetric,[18] fluorescence,[19,20] and chemiresistors.[7,14,17,21–51] A good example of chemiresistors is the pioneering work of Lewis and co-workers, who utilized various carbon black/polymer composite films for sensing VOCs by monitoring changes in the resistance of these films in the presence of vapor analytes.[9] Since then, several groups have studied different types of nanostructures for sensing VOCs and gases. Some examples include semiconductor[41] and metal nanowires,[43,49] carbon nanotubes,[40,52,53] polymer nanowires,[50] and nanoparticles.[14,21,37,54]

Films of metal nanoparticles protected with organic ligands, known as monolayer-protected clusters (MPCs), have been recently reported for sensing VOCs[17,33,39,44,51,55,56] as well as gas analytes.[31,54,56–58] MPCs consist of a metal nanoparticle core surrounded by a self-assembled monolayer shell, which is usually organomercaptans. Wohltjen and Snow first showed that the conductivity of drop-cast films of octanethiolate-coated Au MPCs changes in the presence of various VOCs, including toluene, tetrachloroethylene, 1-propanol, and water.[45] Later, reports examined drop-cast films of MPCs functionalized with aromatic thiols,[26,48] ethylene oxide thiols,[27] and thienyl groups.[21] Others have studied films of MPCs chemically linked by metal ion–carboxylate bridges,[37,47] crown ethers,[59] hydrogen bonding,[14,29] dithiols,[29,30] or dendrimers.[34–36,42,51] The conductivity of alkylamine-stabilized Au MPCs has been shown to respond to sulfur-containing

*Address correspondence to f.zamborini@louisville.edu.

Received for review February 26, 2008 and accepted June 16, 2008.

Published online July 22, 2008.
10.1021/nn800109q CCC: $40.75

analytes.[23] Recently, our group used microscale films of Au MPCs for sensing VOCs[55] and thiolate-[58] or alkylamine[54]-coated Pd or Pd alloy MPCs for H_2 gas sensing. Others have used microscale nanoparticle-based sensors[60] and MPCs for sensing CO_2,[57] NO_2,[56] NH_3,[31] and CO[31] gases. Very recently, Raguse and co-workers inkjet-printed Au MPCs onto a microelectrode for sensing organic vapors dissolved in aqueous electrolyte.[61]

The conductivity of metal (usually Au) MPC films occurs by an electron hopping mechanism,[39,47,62–64] which depends on the separation between metal cores in the film and the dielectric of the surrounding medium. When VOCs interact with the film, both variables can be altered, but a decrease in conductivity usually occurs due to an increase in the cluster-to-cluster distance upon vapor-induced swelling. In some cases, the conductivity of the films increased in the presence of alcohols or water,[29,45,48] but it is not clear if this was due to an increase in the dielectric properties of the medium, film contraction (reduced cluster spacing), or film impurities.[65]

It has been determined that film flexibility is important for high sensitivity through the swelling mechanism, and linking provides stability to MPC films.[33,55] The selectivity for different vapors has been altered by using various types of organic shells or linkers between the clusters.[14,21,26,27,32,33,47] This causes differences in the extent of vapor phase partitioning and film swelling, depending on the functionality of the MPCs and the characteristics of the analyte. Discrimination between vapors is possible using sensor arrays comprising MPCs containing different functionalities and principle component analysis,[14] but this is more challenging in complex samples. MPCs have also been used as chemiresistive detectors for GC,[24] which allows multianalyte detection by separation of the sample into the individual components prior to analysis,[66] and with quartz crystal microbalance (QCM) sensors.[13,29,47]

This paper describes the first use of films of surfactant-stabilized Au and AuAg nanoparticles (NPs) for chemiresistive sensing of VOCs. The particles were chemically synthesized in the presence of tetraoctylammonium bromide (TOABr), drop-cast deposited between a pair of electrodes, and then tested for chemiresistive responses to different VOCs. In comparison to the more common alkanethiolate-coated Au MPCs (hexanethiolates in this paper), films of TOABr-coated Au NPs sense by a different mechanism, are much more sensitive, and have greater long-term stability. Incorporating Ag into the nanoparticle, to form AuAg alloy NPs, leads to altered selectivity, but the sensitivity decreases significantly. Importantly, this shows that the metal core plays a role in the sensing behavior other than just as a conductive medium, which has not been given much attention.[31] Because of their high sensitivity to polar vapors, we believe these sensors show promise for the detection of alcohols, such as in breathalyzers,[1,67] distilleries,[68] or vapor fed direct methanol fuel cells (DMFC).[69,70]

RESULTS AND DISCUSSION

Electronic Properties of Films of TOABr Au and C6S Au. Figure 1A shows cyclic voltammograms (CVs) of solid-state films of tetraoctylammonium bromide (TOABr) only, 4.1 nm average diameter TOABr-stabilized Au NPs, and 1.6 nm average diameter hexanethiolate-coated (C6S) Au MPCs, drop-cast deposited across two Au electrodes separated by a 23 μm gap. The film of C6S Au MPCs shows an increase in current with voltage that retraces itself on the forward and reverse scan, which is consistent with ohmic behavior of the film and an electron hopping process as observed previously.[47,62–64] The film of TOABr only and TOABr-stabilized Au NPs, on the other hand, display current on a similar order of magnitude, but there is significant hysteresis in the current on the forward and reverse scans. This is associated with capacitive charging arising from the presence of TOA^+ and Br^- ions in the film. The capacitive charging is larger for films of TOABr only compared to TOABr-stabilized Au NPs, and the latter shows pseudo-ohmic behavior. The presence of the Au NPs in the TOABr ma-

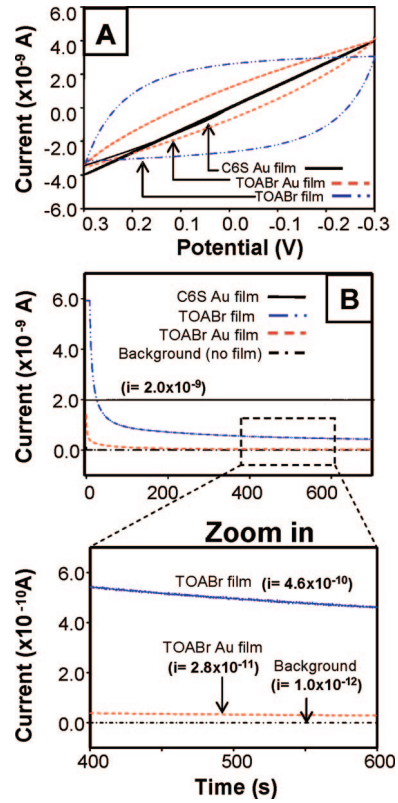

Figure 1. (A) Cyclic voltammograms (CVs) from −0.3 to 0.3 V of films of C6S Au MPCs, TOABr Au, and TOABr only drop-cast deposited between two electrodes separated by a 23 μm gap. (B) Chronoamperometry (CA) plots at −0.3 V of films of C6S Au, TOABr, TOABr Au, and background (no film) under N_2 for a period of 700 s. An expanded plot from 400 to 600 s is shown below frame B.

trix has a large affect on the behavior of TOABr only. Figure 1B shows current *versus* time plots of films of C6S Au MPCs, TOABr only, TOABr Au NPs, and background (no film) held at −0.3 V and exposed to N_2 for 800 s. The current through the film of C6S Au remains stable at 2.0×10^{-9} A with time, consistent with an electron hopping process, while that of TOABr and TOABr Au NPs decreases exponentially with time and eventually stabilizes at approximately 460 and 28 pA, respectively, after 600 s (see expanded plot below frame B in Figure 1). The background current of the device with no film deposited is about 1 pA. The exponential decrease in current with time is characteristic of capacitive charging in the film of both TOABr and TOABr Au NPs; however, the film of TOABr Au NPs decreases faster and stabilizes at a much lower current, again showing that the presence of Au in the TOABr affects the charging behavior.

The data in Figure 1 suggest an electron hopping process for films of C6S Au MPCs and capacitive charging as the dominant current source in films of TOABr and TOABr Au NPs. In addition, films of TOABr and TOABr Au NPs could support Faradaic electrochemical reactions (the origin is unknown), and films of TOABr Au NPs could conduct by electron hopping provided the interparticle distance is small enough. We estimated the number of TOABr ligands per Au NP in the film and obtained scanning electron microscopy (SEM) images to observe the film morphology and NP density, in order to determine if electron hopping is possible within the films. On the basis of the TOABr:Au ratio during synthesis and the diameter of the Au NPs (~4 nm), we estimate a 1200:1 TOABr:Au NP ratio. This is equivalent to approximately 3 to 4 monolayers of TOABr molecules surrounding each Au NP, considering that ~326 C6S molecules form a monolayer around a Au NP of the same size.[71] This is a low estimate, though, since TOABr molecules are more open and would not pack as well as C6S. This large estimated amount of TOABr per Au NP would likely lead to interparticle distances too large for electron hopping, assuming that the TOABr and Au NPs are homogenously mixed throughout the film.

Figures S1 and S2 (Supporting Information) show SEM images of films of C6S Au MPCs and TOABr Au NPs, respectively, to compare their morphology and nanoparticle packing density. The SEM images of films deposited in the same manner as in the sensing experiments (shown later) and Figure 1 are shown in frames A−C. The thickness of these films prevented us from resolving individual nanoparticles or their interparticle spacing. SEM images of 10-fold diluted films (frames D−F) show more details. The C6S Au MPCs are on the order of 1−3 nm in diameter and exhibit dense packing throughout the film, with the exception of some small pits. This is consistent with previous results, ohmic behavior, and an electron hopping process. The TOABr

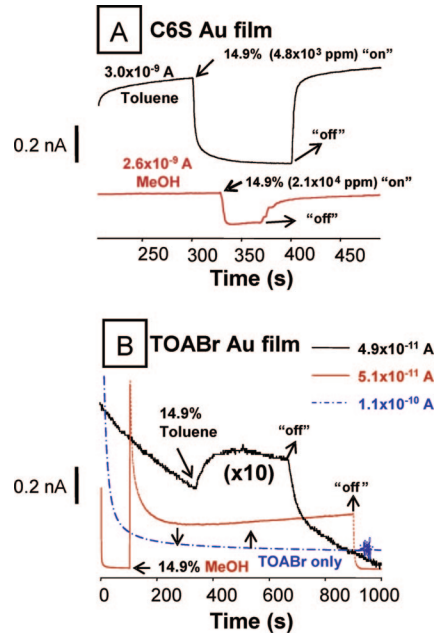

Figure 2. Chronoamperometry (CA) plots at −0.3 V for films of (A) C6S Au MPCs exposed to 14.9% toluene (Tol) and methanol (MeOH) as indicated, (B) TOABr Au NPs exposed to 14.9% MeOH and Tol, and TOABr only exposed to 14.9% MeOH. The plots are offset for clarity, and the response to Tol in (B) is expanded by 10. The currents listed in the figure are the baseline currents immediately before exposing to the vapor.

Au NPs are on the order of 4−5 nm in diameter, and the overall morphology is characterized by large circular rings and other shaped aggregates of densely packed Au NPs surrounded by large micron-sized empty regions that are likely occupied with TOABr. This suggests that the Au NPs and TOABr are not homogenously mixed throughout the film, preventing a conclusive determination of whether electron hopping can occur or not. On one hand, the large micron-sized empty regions would definitely prevent electron hopping through the film. On the other hand, if a densely packed aggregate of Au NPs crossed the electrode gap, there could be a small contribution from electron hopping.

In summary, films of C6S Au MPCs conduct by electron hopping, while films of TOABr are purely capacitive. Films of TOABr Au NPs also exhibit capacitive charging associated with the TOA^+ and Br^- ions, but the addition of Au NPs clearly alters the charging behavior and electron hopping may also occur through densely packed aggregates of Au NPs spanning the electrode gap.

Response of TOABr Au and C6S Au Films to VOCs. Figure 2A,B show chronoamperometry (CA) plots (current *versus* time) for a film of C6S Au, TOABr Au, and TOABr only exposed to 14.9% toluene (Tol) and methanol (MeOH) over time. The beginning of the plot and vapor "off" (or second arrow) correlates with exposure to 100% N_2, and vapor "on" (or first arrow) correlates with exposure to the vapor at the percent indicated in N_2 carrier gas.

The sensing behavior of the two films is very different in three ways. First, the current passing through the film of C6S Au MPCs decreases in the presence of 14.9% toluene and 14.9% methanol but increases for the film of TOABr Au NPs. Second, the film of C6S Au MPCs is more sensitive to Tol (nonpolar vapors) over MeOH, while the film of TOABr Au is more sensitive to MeOH (polar vapors) over Tol. Third, the profile of the current−time plot is different. In the case of the film of C6S Au MPCs, the current decreases with time to a stable value in the presence of the VOC and then returns back to the baseline in the presence of N_2. In contrast, the current through the film of TOABr Au spikes up rapidly, increasing from 5.1×10^{-11} to 1.0×10^{-9} A in the first 5 s of exposure to 14.9% MeOH and then decreases and stabilizes at $\sim 4.0 \times 10^{-10}$ A in ~100 s before returning to the baseline in 100% N_2. As a control, the current through the film of TOABr only does not respond to VOCs (MeOH in Figure 2B), showing that the presence of the Au NPs in the film is necessary for sensing.

The decrease in current in the presence of VOCs for the film of C6S Au MPCs (Figure 2A) has been previously explained by considering the electron hopping conductivity equation used to describe electron transport through these films:[62]

$$\sigma_{EL}(\delta_e, T) = \sigma_0 \exp[-\beta_d \delta_e] \exp[-E_a / RT] \qquad (1)$$

where σ_{EL} is the conductivity of the MPC film, σ_0 is a pre-exponential tunneling factor, δ_e is the distance between particles, β_d is a quantum mechanical tunneling factor, R is the ideal gas constant, T is the temperature, and E_a is the activation energy barrier which uncharged particles need to overcome in order to be positively or negatively charged during electron transport. E_a is expressed as follows:[48]

$$E_a \approx e^2 / 4\pi\epsilon_r\epsilon_0 r \qquad (2)$$

where e is the charge of an electron, ϵ_0 and ϵ_r represent the vacuum permittivity and relative permittivity of the dielectric medium surrounding the metal nanoparticle, respectively, and r is the radius of the nanoparticles. In short, these two equations show that electron hopping conductivity is strongly influenced by the metal nanoparticle edge-to-edge distance (δ_e) in the film and the dielectric properties of the medium (ϵ_r). The decrease in current is explained by an increased nanoparticle spacing as the VOC (Tol or MeOH) partitions into the film, causing it to swell. Since Tol is nonpolar and the MPCs are nonpolar, the partition coefficient for Tol is larger than that for MeOH, which leads to a signal approximately 3 times larger, even though the concentration (in ppm) is 5 times smaller than that of MeOH (Figure 2A). Also, an increase in the dielectric constant of the medium in the case of methanol may decrease E_a and counteract the swelling effect.[26] The sensing mechanism for these types of films has recently been described theoretically in detail by Zellers and coworkers.[39]

The electron hopping equation may or may not apply when considering the increase in current in the presence of VOCs for the film of TOABr Au NPs. As shown in Figure 1, most of the current is dominated by ion flow during capacitive charging. One possible sensing mechanism is that the vapor molecules solvate the film, which leads to an increase in capacitance and ion mobility, decrease in solution resistance, and corresponding increase in current. This is reasonable, and the response to MeOH in Figure 2B shows an initial current transient consistent with this mechanism. The current does not increase similarly for films of TOABr only, though, showing that the Au NPs play a major role in the sensing mechanism. The Au NPs could either facilitate ion transport through the film, which is enhanced by the presence of vapor molecules, or they may play a direct role in electron transport by forming more conductive pathways through the film in the presence of vapor molecules. This could involve rearrangement of the film structure or morphology by movement of the Au NPs in the film. Alternatively, Faradaic electrochemical reactions occurring could be enhanced by the presence of vapor molecules, the details of which are unclear. All of these possibilities are speculation at this point. Future experiments will be designed to determine the mechanism conclusively.

Other groups have observed increased conductivity for Au MPC films in the presence of polar vapors.[26,29,45,48] For example, nonpolar C8 Au MPCs drop-cast deposited on interdigitated electrodes,[45] alkanethiols functionalized with OH terminal groups,[26,48] and Au clusters linked by dithiol bridges[29] displayed increased conductivity upon exposure to water and IPA, EtOH and MeOH, and MeOH and water, respectively. In these cases, conductivity occurs by electron hopping; therefore, the increase in current could be due to film contraction or an increase in the dielectric. Recently, Guo *et al.* showed that the presence of TOABr impurities in dithiol-linked Au MPC films remaining after the synthesis led to an increased conductivity upon exposure to water vapor.[65] They concluded that water solvates the film, leading to enhanced ionic conductivity. Carbon films modified with Na_2CO_3 also showed enhanced conductivity above 31% relative humidity due to improved ionic conductivity or capacitive charging.[72] Our sensing mechanism could be similar as described above, but we cannot completely rule out possible contributions from direct electron transport and Faradaic reactions at this time.

Figure 3 shows the chemiresistive response of devices coated with films of TOABr Au NPs and C6S Au MPCs to MeOH, EtOH, IPA, and Tol at vapor concentrations ranging from 14.9 to 0.27% saturation in N_2 carrier

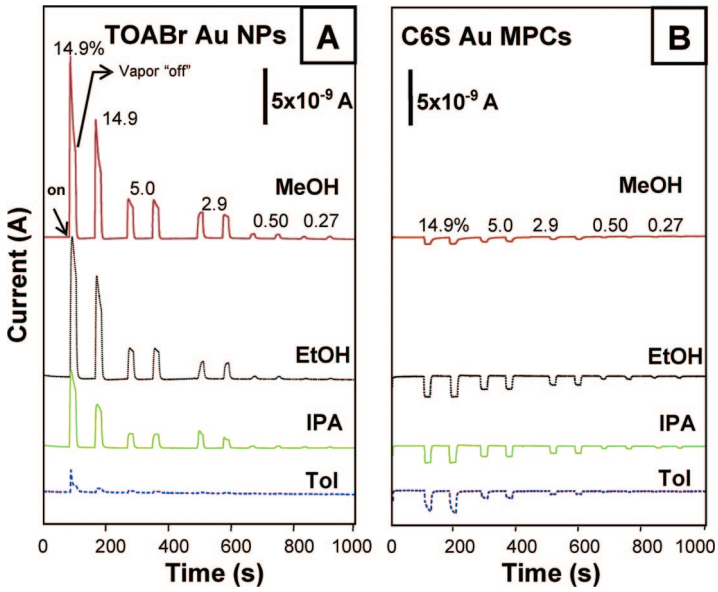

Figure 3. CA plots for films of (A) TOABr Au and (B) C6S Au exposed to methanol (MeOH), ethanol (EtOH), 2-propanol (IPA), and toluene (Tol) from 14.9 to 0.27% vapor concentration. Response profiles are offset for comparison.

gas. The results are similar to those in Figure 2; the film of TOABr Au has an opposite response direction and larger response, especially to polar vapors. Both films give quantitative responses.

Figure 4 shows the chemiresistive response of devices coated with films of TOABr Au NPs and C6S Au MPCs to the same vapors in Figure 3 at concentrations ranging from 0.27 to 0.04%. The asterisk (*) in Figure 4A indicates that the data for the TOABr Au film at 0.27% vapor saturation were acquired separately but placed in the same plot for comparison purposes. All vapors are detected with TOABr Au films at concentrations as low as 0.04% saturation, while MeOH is barely detected at 0.11% and EtOH, IPA, and Tol are not detected below 0.27% with C6S Au MPC films. The different sensing mechanism for the TOABr Au NP films compared to the common swelling mechanism for alkanethiol-coated Au MPC films clearly leads to higher sensitivity. One of the reasons is the extremely low baseline currents, which are close to the background current of the device (Figure 1B). The presence of the VOC acts as a switch, turning on the current well above the low baseline level. This type of positive read-out device is usually more sensitive compared to negative read-out devices like those incorporating C6S Au MPCs.

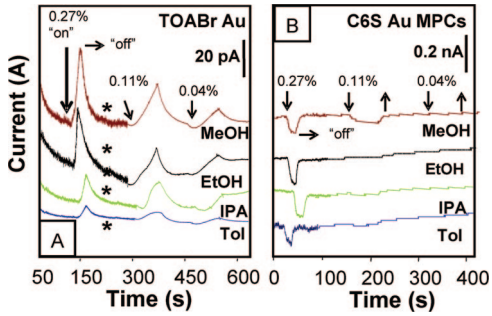

Figure 4. CA plots for films of (A) TOABr Au and (B) C6S Au exposed to methanol (MeOH), ethanol (EtOH), 2-propanol (IPA), and toluene (Tol) from 0.27 to 0.04% vapor concentration. Response profiles are offset for comparison.

Figure 5A,B shows calibration curves plotting the % response[73] *versus* the percent saturation of the vapor (P/P_0) for a device containing a film of TOABr Au NPs and C6S Au MPCs, respectively. Films of TOABr Au exhibit much larger responses compared to films of C6S. For example, at ~15% saturation, responses to IPA, EtOH, and MeOH are all above 100% for the film of TOABr Au, but below (−)10% for the film of C6S Au MPCs. At 15% saturation, the response to toluene is about 40% for TOABr Au as compared to (−)15% for C6S Au MPCs. The negative sign in the response for C6S Au indicates a decrease in current. All of the curves are fairly linear at low concentrations, and the sensor response saturates at higher concentrations, but at different values depending on the type of film and the vapor. This occurs because the VOCs have different vapor pressures, so the concentrations are different at different levels of saturation. The vapor pressure follows the trend of MeOH (0.142) > EtOH (0.073) > IPA (0.046) > Tol (0.032) at 22 °C, leading to concentrations of 57, 29, 18, and 13 ppm at 0.04% for MeOH, EtOH, IPA, and Tol, respectively, for example. Table S1 (Supporting Information) provides all of the percent responses obtained at various concentrations (in % saturation and ppm) for the two devices shown in

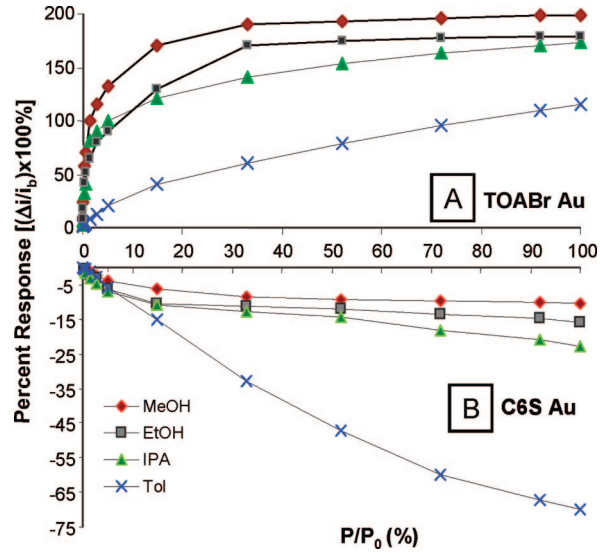

Figure 5. Calibration curves of the percent % response *versus* vapor concentration in % saturation for a device with a film of (A) TOABr Au NPs and (B) C6S Au MPCs.

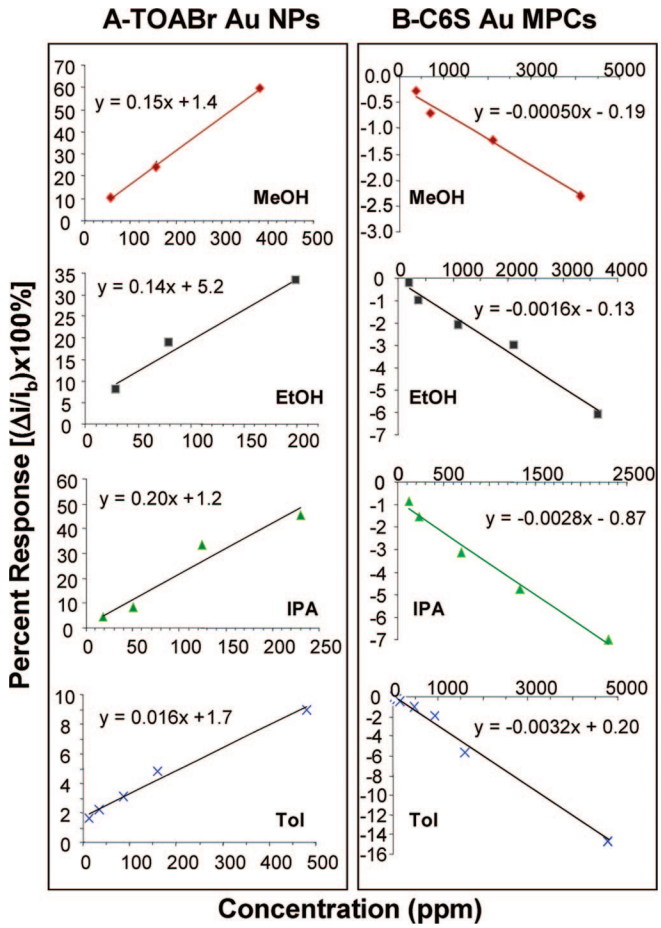

Figure 6. Calibration curves plotting percent response *versus* vapor concentration in ppm in the linear range for films of (A) TOABr Au NPs and (B) C6S Au MPCs exposed to methanol (MeOH), ethanol (EtOH), 2-propanol (IPA), and toluene (Tol).

Figure 5. Table S2 and Figure S3 (Supporting Information) provide all of the data from three different devices containing TOABr Au and C6S Au MPCs and a corresponding bar chart, respectively.

Figure 6 shows calibration curves for each VOC in the linear regime in terms of concentration (in ppm) obtained from a device containing a film of TOABr Au and C6S Au MPCs.[74] The slopes indicate the higher sensitivity of TOABr Au, but films of C6S Au have a wider range of linearity. Table 1 displays the average slope of the calibration curves obtained in the linear regime from three different devices with the standard deviation and the calculated limit of detection (LOD) from sample 1. The LOD for TOABr Au NP films is 30 to 150 times lower for polar vapors compared to C6S Au films, while the LOD for Tol is similar.

Films of TOABr Au NPs also have greater long-term stability when compared to films of C6S Au MPCs. Figure S4 (Supporting Information) compares the sensing behavior of freshly prepared devices to those that sat out in the laboratory for 12 and 16 months containing films of C6S Au MPCs and TOABr Au NPs, respectively. A drastic 60% reduction in response and decrease in the baseline current from 4.5×10^{-9} to 2.0×10^{-9} A occurs for the device with C6S Au MPCs as compared to a <20% reduction in response and very little change in baseline current for the device with TOABr Au NPs.

TABLE 1. Calibration Curve Data for All Sensing Devices Used in This Study

TOABr Au films	Slope-S1	Slope-S2	Slope-S3	avg	STD	LOD[a]
MeOH	0.151	0.159	0.163	0.158	0.006	2
EtOH	0.143	0.119	0.118	0.127	0.013	12
IPA	0.205	0.207	0.194	0.202	0.007	3
Tol	0.0155	0.0160	0.0153	0.0156	0.0004	37

C6S Au films	Slope-S1	Slope-S2	Slope-S3	avg	STD	LOD[a]
MeOH	−0.00050	−0.00052	−0.00059	−0.00054	0.00005	326
EtOH	−0.0016	−0.0017	−0.0014	−0.0015	0.0001	242
IPA	−0.0028	−0.0036	−0.0026	−0.0030	0.0005	106
Tol	−0.0032	−0.0028	−0.0030	−0.0030	0.0002	48

[a]Calculated by multiplying the standard deviation (at ~3 times the LOD) by 3.3 and dividing by the slope for sample 1 only.

Response of TOABr AuAg NPs to VOCs. To alleviate the high cost of Au, we synthesized TOABr-stabilized Ag NPs and measured the response to various VOCs, hoping for similar results. Surprisingly, although the films were conductive, they did not exhibit an appreciable response to any VOCs. This could be due to the higher propensity for Ag to air oxidize compared to Au, which is well-known, but has not been confirmed spectroscopically for these materials by our group. We did observe that TOABr Ag NPs precipitate within a few hours, whereas TOABr Au NPs are stable. To improve the stability while lowering the overall cost, we synthesized TOABr AuAg alloy NPs with ratios of 3:1, 1:1, and 1:3 Au:Ag and tested their chemiresistive sensing properties. Figure S5 (Supporting Information) shows UV−vis spectra of these solutions, which are consistent with the approximate compositions.

Figure 7 shows the chemiresistive response for films of pure Au NPs and 3:1, 1:1, and 1:3 AuAg TOABr alloy NPs exposed to 5.0% Tol and IPA. The figure also displays the selectivity for IPA over Tol obtained from the relation of their responses divided by the concentration (in ppm) as follows:

$$\alpha = R_{IPA} \times C_{IPA}^{-1} / R_{Tol} \times C_{Tol}^{-1} \quad (3)$$

where R is percent response and C is the concentration in ppm. Unfortunately, the presence of Ag in the film greatly reduces the sensitivity. For example, the percent response for films of TOABr AuAg with (Au:Ag) mole ratio of (1:0), (3:1), (1:1), and (1:3) to 5.0% IPA vapor is 87.2, 50.1, 9.5, and 0.7%, respectively. The values are 18.6, 13.2, 0.5, and 0.0 for Tol. This decrease in response with increasing Ag content in the alloy occurs for all of the VOCs (Table S3, Supporting Information). The selectivities for IPA/Tol are 3.2, 2.6, 13.5, and infinity (∞) at

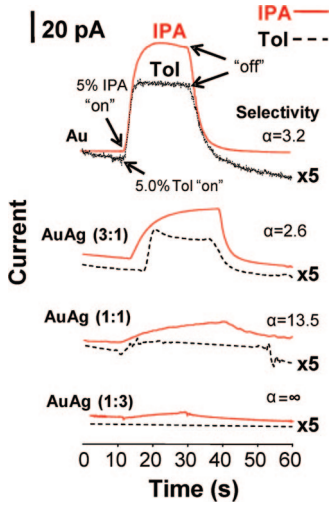

Figure 7. CA plots for films of TOABr Au and TOABr AuAg with Au:Ag ratios of (3:1), (1:1), and (1:3) exposed to 5.0% 2-propanol (IPA) and toluene (Tol).

5.0% saturation for AuAg films with ratios 1:0, 3:1, 1:1, and 1:3, respectively. This shows that the response to Tol decreases more rapidly compared to that for IPA with increasing Ag content, making the sensor more selective to polar vapors. On the other hand, the selectivity among polar vapors (MeOH, EtOH, and IPA) is similar. For instance, selectivity values for IPA/MeOH are 2.3, 2.9, 1.2, and 1.5 for AuAg films with ratios of 0:1, 3:1, 1:1, and 1:3, respectively, at 2.9% vapor saturation. The results in Figure 7 are important because they show that the metal plays an important role in the sensing behavior other than simply acting as a conductive pathway. The air oxidation of pure TOABr Ag is likely responsible for its poor sensing properties; however, the more stable and inert film of 3:1 Au:Ag NPs also shows a significant decrease in response compared to pure Au, suggesting that the Ag may play another role in the sensing apart from its potential air oxidation. Detailed compositional and structural characterization is necessary to better understand the effect of the metal in these types of VOC sensors, which has mostly been ignored in the literature. While adding Ag is detrimental in this example, altering the metal composition could lead to improved sensitivity or selectivity for other metal NP-based sensing devices.

CONCLUSIONS

In conclusion, chemiresistive sensor devices designed with films of TOABr-stabilized Au NPs have several benefits for VOC sensing compared to those using films of C6S Au MPCs. The sensing mechanism is not fully understood but involves changes in capacitive charging and also possibly changes in electron hopping or Faradaic reactions, as opposed to changes in electron hopping only. This leads to an opposite response direction and 30−150 times lower LOD, depending on the vapor. In addition, films of TOABr Au are more stable over a 16 month period. Chemiresistors containing films of AuAg alloy NPs would be reduced in cost, but the sensitivity decreases dramatically with increasing Ag content, although the selectivity of alcohols over Tol is improved. The simple construction, low cost (due to very small quantities of metal needed), stability, durability, high sensitivity, fast response, reversibility, and easy batch production are appealing attributes that may lead to practical uses for these devices, which respond to lower EtOH concentrations when compared to a commercial breathalyzer.[75] In future experiments, we will vary the surfactant and metal in order to optimize the sensors for a specific application and test the devices under real-world conditions.

METHODS

Chemicals. Sodium borohydride (99%), tetraoctylammonium bromide (99%), toluene (99.9%), 2-propanol (99.9%), ethanol (200 proof), methanol (99.9%), dichloromethane (99%), acetone, and acetonitrile (99%) were purchased from VWR Scientific Products. Hexanethiol (96%) and $AgC_2F_3O_2$ were purchased from Aldrich Chemical Co., and $HAuCl_4 \cdot 3H_2O$ was synthesized from metallic Au. Barnstead Nanopure water (17.8 MΩ · cm) was employed for all aqueous solutions.

Synthesis of Hexanethiolate-Coated Au MPCs. Hexanethiolate-coated gold monolayer-protected clusters (C6S Au MPCs) were synthesized according to the Brust reaction;[76] 2.40 g of $HAuCl_4$ was dissolved in 25 mL of water, and 4.89 g of TOABr was dissolved in 150 mL of toluene. The two solutions were combined and stirred until all of the $AuCl_4^-$ transferred into the toluene phase. The toluene phase was separated, and 2.60 mL of hexanethiol, corresponding to a 3:1 thiol:Au ratio, was added to the toluene and stirred until the solution became colorless. The solution was cooled to ~0 °C using an ice bath, and a 10-fold excess of $NaBH_4$ (2.30 g in 10 mL of water) was added to the toluene solution with stirring. The solution turned black within a few seconds, indicating the formation of metallic Au MPCs. Ten milliliters of additional water was added and the solution stirred overnight. The toluene layer was separated and removed by rotary evaporation. The remaining black sludge was suspended in 200 mL of acetonitrile and collected by filtration on a glass fritted Büchner funnel. The black solid product was washed with an additional 250 mL of acetonitrile and thoroughly dried before collecting. Au MPCs prepared this way are 1.6 ± 0.4 nm average diameter according to literature.[71] Scanning electron microscopy (SEM) images (Figure S1, Supporting Information) show Au MPCs in the 1−3 nm diameter range, which is consistent with previous results.

Synthesis of TOABr-Coated Au and AuAg Nanoparticles. Tetraoctylammonium bromide (TOABr)-coated Au nanoparticles (NPs) were synthesized in an identical manner as the C6S Au MPCs, except the hexanethiol was not added.[77,78] Briefly, 0.06 g of $HAuCl_4$ was dissolved in 25 mL of water, and 0.12 g of tetraoctylammonium bromide (TOABr) was dissolved in 100 mL of toluene. The two solutions were combined and stirred until all of the $AuCl_4^-$ transferred into the toluene phase. The solution turned a dark wine red after a 10-fold excess of $NaBH_4$ with respect to Au was added to the toluene solution with stirring. The TOABr Au NPs prepared this way are 4.1 ± 0.8 nm based on atomic force microscopy images. The synthesis of TOABr AuAg nanoparticles followed the same procedure as described above but with the addition of $HAuCl_4$ and $AgC_2F_3O_2$ salt (dissolved in toluene) in the appropriate ratio (3:1, 1:1, and 1:3 Au:Ag).

Film Deposition and Treatment. TOABr-stabilized Au NPs are insoluble when isolated as a powder.[77] Thus, after reduction and

separation from the water phase, the toluene solution containing the particles was reduced to ~50 mL by rotary evaporation, filtered with a microdisc filter (acrodisc, 2 μm PTFE membrane) to remove insoluble materials, and then used from solution. A film of TOABr Au NPs was formed across two Au electrodes separated by 23 μm by drop-cast deposition using 2 drops of a ~0.6 mg/mL solution of TOABr Au NPs (in terms of Au). Films of C6S Au MPCs were drop-cast deposited similarly from a ~20 mg/mL toluene solution. The electrodes were microfabricated in a clean room facility following conventional photolithography, sputtering, and lift off protocols as described previously.[55] The films were allowed to dry and further used for conductivity and sensing measurements.

Vapor Sensing. Vapor sensing experiments were performed by monitoring film current with time using a CH Instruments 660A electrochemical workstation operating in chronoamperometry mode with a two electrode setup as described previously.[55] Measurements were made at room temperature and atmospheric pressure. The current was monitored with time, while a −0.3 V potential was applied between the two electrodes and the sample was exposed to alternating flow of pure N_2 and different concentrations of vapor/N_2. A range of concentrations from 0.04 to 100% VOCs was obtained by varying the flow over a total flow of ~9500 mL/min and by the use of flow meters located between the sample and gas cylinders. The testing of a commercially available breathalyzer (AlcoHAWK ABI) required a larger total flow of 11 618 mL/min as suggested by the company.

Microscopic Characterization. The sample for AFM analysis was prepared as follows. A Si/SiO_x sample was cleaned by immersing in a freshly prepared piranha solution (3:1 H_2SO_4/30%H_2O_2) for 15 min in order to remove organic impurities (**Caution**: piranha solution is a powerful oxidizing agent and reacts violently with organic compounds), rinsed with water, and dried under N_2. The sample was then functionalized with (3-mercaptopropyl)trimethoxysilane (MPTMS) by immersing it into a solution containing 20 mL of 2-propanol (IPA), 100 μL of MPTMS, and ~2 drops of nanopure water. The solution was kept warm on a hot plate at ~30 °C for 20 min. The sample was removed, thoroughly rinsed with IPA, and dried under N_2. A solution of TOABr Au NPs was diluted in toluene by a factor of 1000 and drop-cast deposited onto the Si/SiO_x/MPTMS sample. The sample was rinsed thoroughly with IPA and dried under N_2 before imaging with a Veeco Digital Instruments Nanoscope 3A Multimode scanning probe microscope (Santa Barbara, CA) operating in tapping mode using a Si tip. The average diameter of the TOABr Au was determined based on cross-sectional height analysis of 30 nanoparticles (Figure S6, Supporting Information).

For scanning electron microscopy (SEM) analysis, films of TOABr Au nanoparticles and C6S Au MPCs were prepared by drop-cast deposition between Au electrodes following the same protocol as with the sensing samples and by deposition from solutions diluted by a factor of 10. SEM images (Figures S1 and S2, Supporting Information) were obtained with a Carl Zeiss SMT AG SUPRA 35VP field emission scanning electron microscope (FESEM) operating at an accelerating voltage of 20.00 kV and using an in-lens ion annular secondary electron detector.

Spectroscopic Characterization. UV−vis spectra of TOABr-stabilized NPs in toluene solution were obtained immediately after the synthesis with a Varian Cary 50 spectrometer to qualitatively confirm the composition of the Au, Ag, and AuAg alloy NPs. The concentration was chosen to reach an approximate absorbance of 1.0 at 300 nm.

Acknowledgment. We gratefully acknowledge the National Science Foundation (CHE-0518561) and the Kentucky Science and Engineering Foundation (1032-RDE-008) for support of this research. We thank Grzegorz W. Sławiński from the Department of Chemistry at the University of Louisville for obtaining SEM images, and Kevin M. Walsh, Mark M. Crain, and Ana Sanchez from the Department of Electrical and Computer Engineering at the University of Louisville for use of the clean room to microfabricate the electrode devices.

Supporting Information Available: Scanning electron microscopy (SEM) images of films of C6S Au MPCs and TOABr Au NPs, tables showing sensing data for all devices in this study, bar charts comparing sensing behavior of C6S Au MPCs and TOABr Au NPs, comparison between sensor stability of devices containing C6S Au MPCs and TOABr Au NPs, UV−vis spectra of TOABr Au, Ag, and AuAg alloy NPs in toluene, and atomic force microscopy (AFM) images of TOABr Au NPs. This material is available free of charge *via* the Internet at http://pubs.acs.org.

REFERENCES AND NOTES

1. Mitsubayashi, K.; Yokoyama, K.; Takeuchi, T.; Karube, I. Gas-Phase Biosensor for Ethanol. *Anal. Chem.* **1994**, *66*, 3297–3302.
2. Strike, D. J.; Meijerink, M. G. H.; Koudelka-Hep, M. Electronic Noses−A Mini-Review. *Fresenius J. Anal. Chem.* **1999**, *364*, 499–505.
3. Pejcic, B.; Eadington, P.; Ross, A. Environmental Monitoring of Hydrocarbons: A Chemical Sensor Perspective. *Crit. Rev.* **2007**, *41*, 6333–6342.
4. Finlayson-Pitts, B.; Pitts, J. N. Tropospheric Air Pollution: Ozone, Airborne Toxics, Polycyclic Aromatic Hydrocarbons, and Particles. *Science* **1997**, *276*, 1045–1052.
5. Fitch, J. P.; Raber, E.; Imbro, D. R. Technology Challenges in Responding to Biological or Chemical Attacks in the Civilian Sector. *Science* **2003**, *302*, 1350–1354.
6. Cao, W.; Duan, Y. Breath Analysis: Potential for Clinical Diagnosis and Exposure Assessment. *Clin. Chem.* **2006**, *52*, 800–811.
7. Albert, K. J.; Lewis, N. S.; Schauer, C. L.; Sotzing, G. A.; Stitzel, S. E.; Vaid, T. P.; Walt, D. R. Cross-Reactive Chemical Sensors. *Chem. Rev.* **2000**, *100*, 2595–2626.
8. Gopel, W. Chemical Imaging: I. Concepts and Visions for Electronic and Bioelectronic Noses. *Sens. Actuators, B* **1998**, *52*, 125–142.
9. Lewis, N. S. Comparison between Mammalian and Artificial Olfaction Based on Arrays of Carbon Black−Polymer Composite Vapor Detectors. *Acc. Chem. Res.* **2004**, *37*, 663–672.
10. Pavlou, A. K.; Turner, A. P. F. Sniffing out the Truth: Clinical Diagnosis Using the Electronic Nose. *Clin. Chem. Lab. Med.* **2000**, *38*, 99–112.
11. Yinon, J. Detection of Explosives by Electronic Noses. *Anal. Chem.* **2003**, *75*, 99A–105A.
12. Crooks, R. M.; Ricco, A. J. New Organic Materials Suitable for Use in Chemical Sensor Arrays. *Acc. Chem. Res.* **1998**, *31*, 219–227.
13. Grate, J. W. Acoustic Wave Microsensor Arrays for Vapor Sensing. *Chem. Rev.* **2000**, *100*, 2627–2648.
14. Han, L.; Shi, X.; Wu, W.; Kirk, F. L.; Luo, J.; Wang, L.; Mott, D.; Cousineau, L.; Lim, S. I.-I.; Lu, S.; Zhong, C.-J. Nanoparticle-Structured Sensing Array Materials and Pattern Recognition for VOC Detection. *Sens. Actuators, B* **2005**, *106*, 431–441.
15. Sepaniak, M.; Datskos, P.; Lavrik, N.; Tipple, C. Microcantilever Transducer: A New Approach in Sensor Technology. *Anal. Chem.* **2002**, *74*, 568A–575A.
16. Datskos, P. G.; Sepaniak, M. J.; Tipple, C. A.; Lavrik, N. Photomechanical Chemical Microsensors. *Sens. Actuators, B* **2001**, *76*, 393–402.
17. Yang, C.-J.; Li, C.-L.; Lu, C.-J. A Vapor Selectivity Study of Microsensor Arrays Employing Various Functionalized Ligand Protected Gold Nanoclusters. *Anal. Chim. Acta* **2006**, *565*, 17–26.
18. Rakow, N. A.; Suslick, K. S. A Colorimetric Sensor Array for Odour Visualization. *Nature* **2000**, *406*, 710–713.
19. Yang, J.-S.; Swager, T. M. Fluorescent Porous Polymer Films as TNT Chemosensors: Electronic and Structural Effects. *J. Am. Chem. Soc.* **1998**, *120*, 5321–5322.
20. Drew, S. M.; Janzen, D. E.; Buss, C. E.; MacEwan, D. I.; Dublin, K. M.; Mann, K. R. An Electronic Nose Transducer Array of Vapoluminescent Platinum(II) Double Salts. *J. Am. Chem. Soc.* **2001**, *123*, 8414–8415.

21. Ahn, H.; Chandekar, A.; Kang, B.; Sung, C.; Whitten, J. E. Electrical Conductivity and Vapor-Sensing Properties of ω-(3-Thienyl)alkanethiol-Protected Gold Nanoparticle Films. *Chem. Mater.* **2004**, *16*, 3274–3278.
22. Bekyarova, E.; Kalinina, I.; Itkis, M. E.; Beer, L.; Cabrera, N.; Haddon, R. C. Mechanism of Ammonia Detection by Chemically Functionalized Single-Walled Carbon Nanotubes: *In Situ* Electrical and Optical Study of Gas Analyte Detection. *J. Am. Chem. Soc.* **2007**, *129*, 10700–10706.
23. Briglin, S. M.; Gao, T.; Lewis, N. S. Detection of Organic Mercaptan Vapors Using Thin Films of Alkylamine-Passivated Gold Nanocrystals. *Langmuir* **2004**, *20*, 299–305.
24. Cai, Q.-Y.; Zellers, E. T. Dual-Chemiresistor GC Detector Employing Monolayer-Protected Metal Nanocluster Interfaces. *Anal. Chem.* **2002**, *74*, 3533–3539.
25. Dutta, R.; Hines, E. L.; Gardner, J. W.; Kashwan, K. R.; Bhuyan, M. Tea Quality Prediction Using a Tin Oxide-Based Electronic Nose: An Artificial Intelligence Approach. *Sens. Actuators, B* **2003**, *94*, 228–237.
26. Evans, S. D.; Johnson, S. R.; Cheng, Y. L.; Shen, T. Vapour Sensing Using Hybrid Organic-Inorganic Nanostructured Materials. *J. Mater. Chem.* **2000**, *10*, 183–188.
27. Foos, E. E.; Snow, A. W.; Twigg, M. E.; Ancona, M. G. Thiol-Terminated Di-, Tri-, and Tetraethylene Oxide Functionalized Gold Nanoparticles: A Water-Soluble, Charge-Neutral Cluster. *Chem. Mater.* **2002**, *14*, 2401–2408.
28. Franke, M. E.; Koplin, T. J.; Simon, U. Metal and Metal Oxide Nanoparticles in Chemiresistors: Does the Nanoscale Matter. *Small* **2006**, *2*, 36–50.
29. Han, L.; Daniel, D. R.; Maye, M. M.; Zhong, C.-J. Core-Shell Nanostructured Nanoparticle Films as Chemically Sensitive Interfaces. *Anal. Chem.* **2001**, *73*, 4441–4449.
30. Joseph, Y.; Besnard, I.; Rosenberger, M.; Guse, B.; Nothofer, H.-G.; Wessels, J. M.; Wild, U.; Knop-Gericke, A.; Su, D.; Schlogl, R.; *et al.* Self-Assembled Gold Nanoparticle/Alkanethiol Films: Preparation, Electron Microscopy, XPS-Analysis, Charge Transport, and Vapor-Sensing Properties. *J. Phys. Chem. B* **2003**, *107*, 7406–7413.
31. Joseph, Y.; Guse, B.; Yasuda, A.; Vossmeyer, T. Chemiresistor Coatings from Pt- and Au-Nanoparticle/Nonanedithiol Films: Sensitivity to Gases and Solvent Vapors. *Sens. Actuators, B* **2004**, *98*, 188–195.
32. Joseph, Y.; Krasteva, N.; Besnard, I.; Guse, B.; Rosenberger, M.; Wild, U.; Knop-Gericke, A.; Schlogl, R.; Krustev, R.; Yasuda, A.; *et al.* Gold-Nanoparticle/Organic Linker Films: Self-Assembly, Electronic, and Structural Characterisation, Composition and Vapour Sensitivity. *Faraday Discuss.* **2004**, *125*, 77–97.
33. Joseph, Y.; Peic, A.; Chen, X.; Michl, J.; Vossmeyer, T.; Yasuda, A. New Sensitivity of Networked Gold Nanoparticle Chemiresistors: Importance of Flexibility and Resistivity of the Interlinkage. *J. Phys. Chem. C* **2007**, *111*, 12855–12859.
34. Krasteva, N.; Besnard, I.; Guse, B.; Bauer, R. E.; Mullen, K.; Yasuda, A.; Vossmeyer, T. Self-Assembled Gold Nanoparticle/Dendrimer Composite Films for Vapor Sensing Applications. *Nano Lett.* **2002**, *2*, 551–555.
35. Krasteva, N.; Guse, B.; Besnard, I.; Yasuda, A.; Vossmeyer, T. Gold Nanoparticle/PPI-Dendrimer Based Chemiresistors Vapor-Sensing Properties as a Function of the Dendrimer Size. *Sens. Actuators, B* **2003**, *92*, 137–143.
36. Krasteva, N.; Krustev, R.; Yasuda, A.; Vossmeyer, T. Vapor Sorption in Self-Assembled Gold Nanoparticle/Dendrimer Films Studied by Specular Neutron Reflectometry. *Langmuir* **2003**, *19*, 7754–7760.
37. Leopold, M. C.; Donkers, R. L.; Georganopoulou, D.; Fisher, M.; Zamborini, F. P.; Murray, R. W. Growth, Conductivity, and Vapor Response Properties of Metal Ion-Carboxylate Linked Nanoparticle Films. *Faraday Discuss.* **2004**, *125*, 63–76.
38. Pang, P.; Guo, Z.; Cai, Q. Humidity Effect on the Monolayer-Protected Gold Nanoparticles Coated Chemiresistor Sensor for VOCs Analysis. *Talanta* **2005**, *65*, 1343–1348.
39. Steinecker, W. H.; Rowe, M. P.; Zellers, E. T. Model of Vapor-Induced Resistivity Changes in Gold-Thiolate Monolayer-Protected Nanoparticle Sensor Films. *Anal. Chem.* **2007**, *79*, 4977–4986.
40. Sun, Y.; Wang, H. H. High-Performance, Flexible Hydrogen Sensors that Use Carbon Nanotubes Decorated with Palladium Nanoparticles. *Adv. Mater.* **2007**, *19*, 2818–2823.
41. Sysoev, V. V.; Button, B. K.; Wepsiec, K.; Dmitriev, S.; Kolmakov, A. Toward the Nanoscopic "Electronic Nose": Hydrogen *vs* Carbon Monoxide Discrimination with an Array of Individual Metal Oxide Nano- and Mesowire Sensors. *Nano Lett.* **2006**, *6*, 1584–1588.
42. Vossmeyer, T.; Guse, B.; Besnard, I.; Bauer, R. E.; Mullen, K.; Yasuda, A. Gold Nanoparticle/Polyphenylene Dendrimer Composite Films: Preparation and Vapor-Sensing Properties. *Adv. Mater.* **2002**, *14*, 238–242.
43. Walter, E. C.; Favier, F.; Penner, R. M. Palladium Mesowire Arrays for Fast Hydrogen Sensors and Hydrogen-Actuated Switches. *Anal. Chem.* **2002**, *74*, 1546–1553.
44. Wang, L.-S.; Xiajing, K.; Karuiki, N. N.; Schadt, M.; Wang, G. R.; Rendeng, Q.; Choi, J.; Luo, J.; Lu, S.; Zhong, C.-J. Array of Molecular Mediated Thin Film Assemblies of Nanoparticles: Correlation of Vapor Sensing with Interparticle Spatial Properties. *J. Am. Chem. Soc.* **2007**, *129*, 2161–2170.
45. Wohltjen, H.; Snow, A. W. Colloidal Metal-Insulator-Metal Ensemble Chemiresistor Sensor. *Anal. Chem.* **1998**, *70*, 2856–2859.
46. Woodka, M. D.; Brunschwig, B. S.; Lewis, N. S. Use of Spatiotemporal Response Information from Sorption-Based Sensor Arrays to Identify and Qualify the Composition of Analyte Mixtures. *Langmuir* **2007**, *23*, 13232–13241.
47. Zamborini, F. P.; Leopold, M. C.; Hicks, J. F.; Kulesza, P. J.; Malik, M. A.; Murray, R. W. Electron Hopping Conductivity and Vapor Sensing Properties of Flexible Network Polymer Films of Metal Nanoparticles. *J. Am. Chem. Soc.* **2002**, *124*, 8958–8964.
48. Zhang, H.-L.; Evans, S. D.; Henderson, J. R.; Miles, R. E.; Shen, T.-H. Vapour Sensing Using Surface Functionalized Gold Nanoparticles. *Nanotechnology* **2002**, *13*, 439–444.
49. Im, Y.; Lee, C.; Vazquez, R. P.; Bangar, M. A.; Myung, N. V.; Menke, E. J.; Penner, R. M.; Yun, M. Investigation of a Single Pd Nanowire for Use as a Hydrogen Sensor. *Small* **2006**, *2*, 356–358.
50. Rahman, A.; Sanyal, M. K. Novel Switching Transition of Resistance Observed in Conducting Polymer Nanowires. *Adv. Mater.* **2007**, *19*, 3956–3960.
51. Krasteva, N.; Fogel, Y.; Bauer, R. E.; Mullen, K.; Joseph, Y.; Matsuzawa, A.; Vossmeyer, T. Vapor Sorption and Electrical Response of Au-Nanoparticle-Dendrimer Composites. *Adv. Funct. Mater.* **2007**, *17*, 881–888.
52. Qi, P.; Vermesh, O.; Grecu, M.; Javey, A.; Wang, Q.; Dai, H.; Peng, S.; Cho, K. J. Toward Large Array of Multiplex Functionalized Carbon Nanotube Sensor for Highly Sensitive and Selective Molecular Detection. *Nano Lett.* **2003**, *3*, 347–351.
53. Snow, E. S.; Perkins, F. K.; Robinson, J. A. Chemical Vapor Detection Using Single-Walled Carbon Nanotubes. *Chem. Soc. Rev.* **2006**, *35*, 790–798.
54. Ibañez, F. J.; Zamborini, F. P. Reactivity of Hydrogen with Solid-State Films of Alkylamine- and Tetraoctylammonium Bromide-Stabilized Pd, PdAg, and PdAu Nanoparticles for Sensing and Catalysis Applications. *J. Am. Chem. Soc.* **2008**, *130*, 622–633.
55. Ibañez, F. J.; Growrishetty, U.; Crain, M. M.; Walsh, K. M.; Zamborini, F. P. Chemiresistor Vapor Sensing with Microscale Films of Gold Monolayer Protected Clusters. *Anal. Chem.* **2006**, *78*, 753–761.
56. Hanwell, M. D.; Heriot, S. Y.; Richardson, T. H.; Cowlam, N.; Ross, L. M., Gas and Vapor Sensing Characteristics of Langmuir-Schaeffer Thiol Encapsulated Gold Nanoparticle Thin Films. *Colloids Surf., A: Phys. Chem. Eng. Aspects* **2006**, 284−285; 311−319.

57. Choi, J.-P.; Coble, M. M.; Branham, M. R.; DeSimone, J. M.; Murray, R. W. Dynamics of CO_2-Plasticized Electron Transport in Au Nanoparticle Films: Opposing the Effects of Tunneling Distance and Local Site Mobility. *J. Phys. Chem. C* **2007**, *111*, 3778–3785.
58. Ibañez, F. J.; Zamborini, F. P. Ozone- and Thermally Activated Films of Palladium Monolayer-Protected Clusters for Chemiresistive Hydrogen Sensing. *Langmuir* **2006**, *22*, 9789–9796.
59. Pompano, R. R.; Wortley, P. G.; Moatz, L. M.; Tognarelli, D. J.; Kittredge, K. W.; Leopold, M. C. Crown Ether-Metal "Sandwiches" as Linking Mechanisms in Assembled Nanoparticle Films. *Thin Solid Films* **2006**, *510*, 311–319.
60. Harnack, O.; Raible, I.; Yasuda, A.; Vossmeyer, T. Lithographic Patterning of Nanoparticle Films Self-Assembled from Organic Solutions by Using a Water-Soluble Mask. *Appl. Phys. Lett.* **2005**, *86*, 034108-1–034108-3.
61. Raguse, B.; Christopher, E. C.; Barton, C. S.; Wieczorek, L. Gold Nanoparticle Chemiresistor Sensor: Direct Sensing of Organics in Aqueous Electrolyte Solution. *Anal. Chem.* **2007**, *79*, 7333–7339.
62. Terrill, R. H.; Postlethwaite, T. A.; Chen, C.-H.; Poon, C.-D.; Terzis, A.; Chen, A.; Hutchison, J. E.; Clark, M. R.; Wignall, G.; Londono, J. D.; et al. Monolayers in Three Dimensions: NMR, SAXS, Thermal, and Electron Hopping Studies of Alkanethiol Stabilized Gold Clusters. *J. Am. Chem. Soc.* **1995**, *117*, 12537–12548.
63. Wuelfing, W. P.; Green, S. J.; Pietron, J. J.; Cliffel, D. E.; Murray, R. W. Electronic Conductivity of Solid-State, Mixed-Valent, Monolayer-Protected Au Clusters. *J. Am. Chem. Soc.* **2000**, *122*, 11465–11472.
64. Zamborini, F. P.; Smart, L. E.; Leopold, M. C.; Murray, R. W. Distance-Dependent Electron Hopping Conductivity and Nanoscale Lithography of Chemically Linked Gold Monolayer Protected Cluster Films. *Anal. Chim. Acta* **2003**, *496*, 3–16.
65. Guo, J.; Pang, P.; Cai, Q. Effect of Trace Residual Ionic Impurities on the Response of Chemiresistor Sensors with Dithiol-Linked Monolayer-Protected Gold (Nano)clusters as Sensing Interfaces. *Sens. Actuators, B* **2007**, *120*, 521–528.
66. Jin, C.; Kurzawsky, P.; Hierlemmann, A.; Zellers, E. T. Evaluation of Multitransducer Array for the Determination of Organic Vapors. *Anal. Chem.* **2008**, *80*, 227–236.
67. Groves, W. A.; Zellers, E. T. Analysis of Solvent Vapors in Breath and Ambient Air with a Surface Acustic Wave Sensor Array. *Ann. Occup. Hyg.* **2001**, *45*, 609–623.
68. Rotariu, L.; Bala, C.; Magerau, V. New Potentiometric Microbial Biosensor for Ethanol Determination in Alcoholic Berverages. *Anal. Chim. Acta* **2004**, *513*, 119–123.
69. Kim, D. W.; Lee, J. S.; Lee, G. S.; Overzet, L.; Kozlov, M.; Aliev, A. E.; Park, Y. W.; Yang, D. J. Carbon Nanotube Based Methanol Sensor for Fuel Cell Application. *J. Nanosci. Nanotechnol.* **2006**, *6*, 3608–3613.
70. Drew, K.; Girishkumar, G.; Vinodgopal, K.; Kamat, P. V. Boosting Fuel Cell Performance with a Semiconductor Photocatalyst: TiO_2/Pt-Ru Hybrid Catalyst for Methanol Oxidation. *J. Phys. Chem. B* **2005**, *109*, 11851–11857.
71. Hostetler, M. J.; Wingate, J. E.; Zhong, C.-J.; Harris, J. E.; Vachet, R. W.; Clark, M. R.; Londono, J. D.; Green, S. J.; Stokes, J. J.; Wignall, G. D.; *et al.* Alkanethiolate Gold Cluster Molecules with Core Diameters from 1.5 to 5.2 nm: Core and Monolayer Properties as a Function of Core Size. *Langmuir* **1998**, *14*, 17–30.
72. Lukaszewicz, J. P.; Skompska, M. A Novel Carbon-Based Ionic Conductor for Humidity Sensor. *Sens. Actuators, B* **2005**, *113*, 970–977.
73. % Response $= (i_r - i_b)/i_b \times 100\% = \Delta i/i_b \times 100\%$, where i_r is the current response and i_b is the baseline current. Current response (i_r) for films of TOABr Au NPs was acquired by measuring the current at the sharpest part of the peak.
74. The line of best fit was not forced through zero. The data points correspond to values within the linear range for each vapor.
75. A device with a film of TOABr Au NPs was compared to a commercially available breathalyzer (AlcoHAWK ABI). The experimental limit of detection of ethanol (ETOH) was 29 and 75 ppm for the TOABr Au NP device and the commercial breathalyzer, respectively.
76. Brust, M.; Walker, M.; Bethell, D.; Schiffrin, D. J.; Whyman, R. Synthesis of Thiol-Derivatised Gold Nanoparticles in a Two-Phase Liquid−Liquid System. *J. Chem. Soc., Chem. Commun.* **1994**, *7*, 801–802.
77. Isaacs, S. R.; Culter, E. C.; Park, J.-S.; Lee, T. R.; Shon, Y.-S. Synthesis of Tetraoctylammonium-Protected Gold Nanoparticles with Improved Stability. *Langmuir* **2005**, *21*, 5689–5692.
78. Fink, J.; Kiely, C. J.; Bethell, D.; Schiffrin, D. J. Self-Organization of Nanosized Gold Nanoparticle. *Chem. Mater.* **1998**, *10*, 922–926.